Demonstration of a cylindrically symmetric second-order nonlinear fiber with self-assembled organic surface layers

Chalongrat Daengngam,[1] Matthias Hofmann,[2] Zhiwen Liu,[3] Anbo Wang,[2] James R. Heflin,[1] and Yong Xu[2,*]

[1]*Department of Physics, Virginia Polytechnic Institute and State University, Blacksburg, VA 24061, USA*
[2]*Department of Electrical and Computer Engineering, Virginia Polytechnic Institute and State University, Blacksburg, VA 24061, USA*
[3]*Department of Electrical Engineering, Pennsylvania State University, University Park, PA 16802, USA*
[*]yong@vt.edu

Abstract: We report the fabrication and characterization of a cylindrically symmetric fiber structure that possesses significant and thermodynamically stable second-order nonlinearity. Such fiber structure is produced through nanoscale self-assembly of nonlinear molecules on a silica fiber taper and possesses full rotational symmetry. Despite its highly symmetric configuration, we observed significant second harmonic generation (SHG) and obtained good agreement between experimental results and theoretical predictions.

©2011 Optical Society of America

OCIS codes: (060.4370) Nonlinear optics, fiber; (190.2620) Harmonic generation and mixing.

References and links

1. G. P. Agrawal, *Nonlinear fiber optics* (Elsevier, Singapore, 2007)
2. B. P. Antonyuk, N. N. Novikova, N. V. Didenko, and O. A. Aktsipetrov, "All optical poling and second harmonic generation in glasses: theory and experiment," Phys. Lett. A **287**(1-2), 161–168 (2001).
3. M. K. Balakirev, V. A. Smirnov, and L. I. Vostrikova, "Photorefractive effect on all optical polling of glass," J. Opt. A, Pure Appl. Opt. **5**(6), S437–S443 (2003).
4. V. Tombelaine, C. Buy-Lesvigne, P. Leproux, V. Couderc, and G. Mélin, "Optical poling in germanium-doped microstructured optical fiber for visible supercontinuum generation," Opt. Lett. **33**(17), 2011–2013 (2008).
5. R. A. Myers, N. Mukherjee, and S. R. J. Brueck, "Large second-order nonlinearity in poled fused silica," Opt. Lett. **16**(22), 1732–1734 (1991).
6. H. An, and S. Fleming, "Second-order optical nonlinearity in thermally poled borosilicate glass," Appl. Phys. Lett. **89**, 181111(1)-181111(3) (2006).
7. A. Canagasabey, C. Corbari, Z. Zhang, P. G. Kazansky, and M. Ibsen, "Broadly tunable second-harmonic generation in periodically poled silica fibers," Opt. Lett. **32**(13), 1863–1865 (2007).
8. V. Pruneri, G. Bonfrate, P. G. Kazansky, D. J. Richardson, N. G. Broderick, J. P. de Sandro, C. Simonneau, P. Vidakovic, and J. A. Levenson, "Greater than 20%-efficient frequency doubling of 1532-nm nanosecond pulses in quasi-phase-matched germanosilicate optical fibers," Opt. Lett. **24**(4), 208–210 (1999).
9. A. Canagasabey, C. Corbari, A. V. Gladyshev, F. Liegeois, S. Guillemet, Y. Hernandez, M. V. Yashkov, A. Kosolapov, E. M. Dianov, M. Ibsen, and P. G. Kazansky, "High-average-power second-harmonic generation from periodically poled silica fibers," Opt. Lett. **34**(16), 2483–2485 (2009).
10. T. Fujiwara, M. Takahashi, and A. J. Ikushima, "Second-harmonic generation in germanosilicate glass poled with ArF laser irradiation," Appl. Phys. Lett. **71**(8), 1032–1034 (1997).
11. C. Corbari, P. G. Kazasky, S. A. Slattery, and N. Nikogosyan, "Ultraviolet poling of pure fused silica by high-intensity femtosecond radiation," Appl. Phys. Lett. **86**, 071106(1)-071106 (3) (2005).
12. A. Okada, K. Ishii, K. Mito, and K. Sasaki, "Phase-matched second-harmonic generation in novel corona poled glass waveguides," Appl. Phys. Lett. **60**(23), 2853–2855 (1992).
13. S. Horinouchi, H. Imai, G. J. Zhang, K. Mito, and K. Sasaki, "Optical quadratic nonlinearity in multilayer corona-poled glass films," Appl. Phys. Lett. **68**(25), 3552–3554 (1996).
14. C.-A. Tsai, J. N. Wang, V. Chao-Wei-Kuo, T. Y. Cheng, W.-R. Liou, and A. Y. Wu, "Enhancement of SHG in fused SiO$_2$ by corona poling under water, water vapor and salty environments," J. Mar. Sci. Technol. **16**, 90–102 (2008).
15. Y. Jiang, P. T. Wilson, M. Downer, C. W. White, and S. P. Withrow, "Second harmonic generation from silicon nanocrystals embedded in SiO$_2$," Appl. Phys. Lett. **78**(6), 766–768 (2001).
16. Y. Yamamoto, H. Nasu, T. Hashimoto, and K. Kamiya, "Second harmonic generation from thermally poled CdS microcrystal-containing glasses," J. Non-Cryst. Solids **281**(1-3), 198–204 (2001).

17. X. Xiao, Q. Liu, G. Dong, and X. Zhao, "Second-order optical nonlinearity in Sb_2S_3 microcrystal doped glasses by electron beam irradiation," Opt. Commun. **274**(2), 456–460 (2007).
18. A. L. Moura, M. T. de Araujo, M. V. D. Vermelho, and J. S. Aitchison, "Improved stability of the induced second-order nonlinearity in soft glass by thermal poling," J. Appl. Phys. **100**(3), 033509 (2006).
19. T. Fujiwara, M. Takahashi, and A. J. Ikushima, "Decay behaviour of second-order nonlinearity in GeO_2-SiO_2 glass poled with UV-irradiation," Electron. Lett. **33**(11), 980–982 (1997).
20. H. Imai, S. Horinouchi, Y. Uchida, H. Yamasaki, K. Fukao, G. Zhang, T. Kinoshita, K. Mito, H. Hirashima, and K. Sasaki, "Time-dependent decay of quadratic non-linearity in corona-poled silicate glass films," J. Non-Cryst. Solids **196**, 63–66 (1996).
21. Y. Xu, A. Wang, J. R. Heflin, and Z. Liu, "Proposal and analysis of a silica fiber with large thermodynamically stable second order nonlinearity," Appl. Phys. Lett. **90**(21), 211110 (2007).
22. Y. Xu, M. Han, A. Wang, Z. Liu, and J. R. Heflin, "Second order parametric processes in nonlinear silica microspheres," Phys. Rev. Lett. **100**(16), 163905 (2008).
23. J. R. Heflin, M. T. Guzy, P. J. Neyman, K. J. Gaskins, C. Brands, Z. Wang, H. W. Gibson, R. M. Davis, and K. E. Van Cott, "Efficient, thermally stable, second order nonlinear optical response in organic hybrid covalent/ionic self-assembled films," Langmuir **22**(13), 5723–5727 (2006).
24. T. A. Birks and Y. W. Li, "The shape of fiber tapers," J. Lightwave Technol. **10**(4), 432–438 (1992).
25. S. Xue, M. van Eijkelenborg, G. W. Barton, and P. Hambley, "Theoretical, numerical, and experimental analysis of optical fiber tapering," J. Lightwave Technol. **25**(5), 1169–1176 (2007).
26. K. Van Cott, M. Guzy, P. Neyman, C. Brands, J. R. Heflin, H. W. Gibson, and R. M. Davis, "P, Neyman, C. Brands, J. R. Heflin, H. W. Gibson, and R. M. Davis, "Layer-by-layer deposition and ordering of low-molecular-weight dye molecules for second order nonlinear optics," Angew. Chem. Int. Ed. **41**(17), 3236–3238 (2002).
27. G. Zhai and L. Tong, "Roughness-induced radiation losses in optical micro or nanofibers," Opt. Express **15**(21), 13805–13816 (2007).
28. Y. Fujii, B. S. Kawasaki, K. O. Hill, and D. C. Johnson, "Sum-frequency light generation in optical fibers," Opt. Lett. **5**(2), 48–50 (1980).
29. M. A. Saifi and M. J. Andrejco, "Second-harmonic generation in single-mode and multimode fibers," Opt. Lett. **13**(9), 773–775 (1988).
30. D. A. Akimov, A. A. Ivanov, A. N. Naumov, O. A. Kolevatova, M. V. Alfimov, T. A. Brisk, W. J. Wadsworth, P. St. J. Russell, A. A. Podshivalov, and A. M. Zheltikov, "Generation of a spectrally asymmetric third harmonic with unamplified 30-fs Cr:forsterite laser pulses in a tapered fiber," Appl. Phys. B **76**, 515–519 (2003).
31. V. Grubsky and J. Feinberg, "Phase-matched third-harmonic UV generation using low-order modes in a glass micro-fiber," Opt. Commun. **274**(2), 447–450 (2007).
32. Y. R. Shen, *The principles of nonlinear optics* (John Wiley and Sons, New Jersey, 1984)
33. M. J. Cho, D. H. Choi, P. A. Sullivan, A. J. P. Akelaitis, and L. R. Dalton, "Recent progress in second-order nonlinear optical polymer and dendrimers," Prog. Polym. Sci. **33**(11), 1013–1058 (2008).
34. B. Brochers, J. Bekesi, P. Simon, and J. Ihlemann, "Submicron surface patterning by laser ablation with short UV pulses using a proximity phase mask setup," J. Appl. Phys. **107**, 063106(1)-063106(4) (2010).
35. A. Rastogi, M. Y. Paik, M. Tanaka, and C. K. Ober, "Direct patterning of intrinsically electron beam sensitive polymer brushes," ACS Nano **4**(2), 771–780 (2010).
36. F. Pan, P. Wang, K. Lee, A. Wu, N. J. Turro, and J. T. Koberstein, "Photochemical modification and patterning of polymer surfaces by surface adsorption of photoactive block copolymers," Langmuir **21**(8), 3605–3612 (2005).
37. U. Wiedemann, K. Karapetyan, C. Dan, D. Pritzkau, W. Alt, S. Irsen, and D. Meschede, "Measurement of submicrometre diameters of tapered optical fibres using harmonic generation," Opt. Express **18**(8), 7693–7704 (2010).

1. Introduction

The advance in silica fiber technology has not only revolutionized modern telecommunications but also created major research disciplines such as nonlinear fiber optics. Yet even after decades of development, research in nonlinear fiber optics remains primarily limited to third-order effects such as four-wave-mixing and optical solitons [1]. This fundamental limitation arises from a simple fact: As an amorphous material with full inversion symmetry, silica glass cannot possess second-order nonlinearity. Consequently, until now it has been very difficult to use silica fiber to realize some of the most important second-order processes including second harmonic generation (SHG) and optical parametric oscillation (OPO).

Recently, a few research groups have developed several methods that aim to overcome the lack of second-order nonlinearity in silica fiber devices. Most such methods are based on poling silica glass using external fields, with examples including optical poling [2,4], electrical poling [5–9], UV poling [10,11], corona poling [12–14], or doping microstructures into fibers [15–17]. However, since all such techniques introduce a preferred direction into silica glass, the induced second-order nonlinearity is thermodynamically unstable and tends to

decay over time [2,18–20]. In contrast to current methods, we have theoretically demonstrated that it is possible to generate significant second-order nonlinearity in a silica fiber by coating it with layers of radially aligned nonlinear molecules [21,22]. The coating process can be accomplished through a layer-by-layer self-assembly, where the alignment of the nonlinear molecules is maintained through electrostatic interaction. As a result, the second-order nonlinearity of the proposed fibers is thermodynamically stable, which cannot currently be achieved by any other means [23]. Furthermore, the proposed fibers can generate significant second-order nonlinear responses despite their full rotational symmetry. In fact, for such fibers, instead of being a hindrance, the high degree of symmetry directly leads to a symmetry-enforced selection rule that can produce quantum entanglement [21,22]. In the present publication, we report the fabrication of such silica-based nonlinear fibers and experimental confirmation of their second-order nonlinearity.
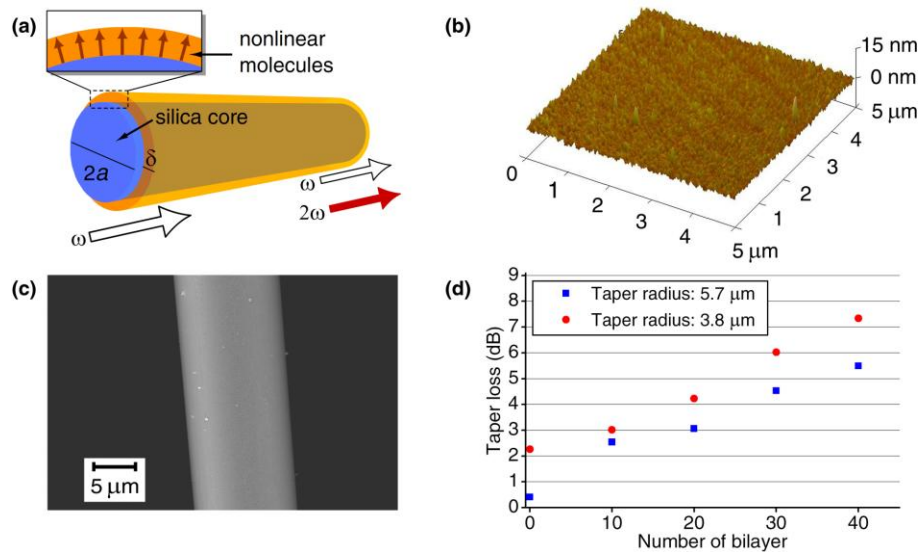
2. Fabrications

Fig. 1. Nonlinear coating on a silica fiber. (a) The schematic structure of nonlinear fiber with full cylindrical symmetry. The radially aligned nonlinear molecules provide a second-order susceptibility tensor dominated by the $\chi^{(2)}_{rrr}$ component. (b) The AFM image of 10-bilayer nonlinear self-assembled film on a planar glass substrate shows highly uniform coating. (c) SEM image of a nonlinear fiber with 10-bilayer coating. (d) The transmission loss of a coated taper at wavelength of 1294 nm was recorded for every 10-bilayer film deposition.

The schematic of the silica-based nonlinear fiber is shown in Fig. 1(a). It consists of a uniform silica core covered by layers of radially aligned nonlinear molecules. The fabrication of such nonlinear fibers begins with pulling silica fiber tapers with diameter in the range of a few microns. (Such a small diameter is necessary in order to achieve strong interaction between the optical field and the nonlinear molecules.) Our taper pulling process is similar to the procedures described in Refs [24]. and [25]. Briefly, we placed a silica fiber between two fiber clamps and used a propane-oxygen flame to heat the fiber. As the glass softens, we slowly pulled the two clamps apart. The pulling speed was precisely controlled by two Newport UTM100CC.1 motion stages, which enabled us to tailor the waist size and the profile of the fiber taper. All fiber tapers in the following discussions were produced using a multimode fiber (50 μm core and 125 μm cladding, Corning ClearCurve OM2), where the taper waist radius ranges from 2.8 to 7.5 μm. Optical transmission of such fiber tapers is typically above 90%.

The next step in the nonlinear fiber fabrication is the self-assembly of radially aligned nonlinear molecules. The coating process is based on a novel hybrid covalent/ionic self-

assembled multilayer technique developed by one of the authors [23]. Briefly, we dipped the fiber taper into a polycationic solution containing poly(allylamine hydrochloride) (PAH) with pH 7.0 and 10 mM concentration, whereupon a monolayer of positively charged PAH film grew uniformly on the negatively charged taper surface. Following PAH deposition, we dipped the fiber sample into an aqueous solution containing nonlinear molecules Procion Brown MX-GRN (PB) at pH 10.5, 5 mg/mL concentration and 0.5 M NaCl added. At this pH, the dichlorotriazine moieties of PB form covalent bonds with the unprotonated amines of PAH. Upon deposition of the sequential PAH layer at pH 7.0, the negatively-charged sulfonates of PB bind electrostatically with the protonated amine groups of PAH. The deposition of each monolayer requires less than two minutes and can be repeated as many times as desired to produce multilayer nonlinear optical films [26].

The nonlinear optical properties of PAH/PB films on planar glass substrate have been studied. It was found that the second-order nonlinear tensor of the film was dominated by the *zzz* component with $\chi_{zzz}^{(2)}$ *= 21 pm/V, approximately two third the value* of LiNbO$_3$ [23]. (The z direction is normal to the planar glass substrate.) Since molecular orientation of the PAH/PB film is maintained through electrostatic and covalent interactions, the nonlinear susceptibility of the film is thermodynamically stable. For example, the self-assembled films exhibit excellent thermal and temporal stability with no decrease of $\chi_{zzz}^{(2)}$ *after a temperature cycles to 150° C for 24 hours or under ambient condition for more than two years [23]. They are also mechanically stable and impervious to immersion in water and* most organic solvents.

Since the thickness of each PAH/PB bilayer is only ~1 nm [23], the nonlinear molecules can conformally coat the silica fiber while maintaining a radial alignment. Figure 1(b) shows an atomic force microscope (AFM) image of 10-bilayer PAH/PB film on a planar glass substrate. As revealed by the AFM image, the PAH/PB film is highly uniform, and the standard deviation of film thickness is only 3 nm. Figure 1(c) shows a scanning electron microscope (SEM) image of a silica fiber taper coated with 10-bilayer PAH/PB film. The SEM image indicates a smooth and uniform nonlinear coating occasionally marred by the presence of dust particles. Since all fiber fabrication was performed outside a clean room, the appearance of dust particles is not unexpected. The transmission loss of the nonlinear fiber taper was monitored throughout the entire self-assembly process. Figure 1(d) shows the measured transmission loss for two nonlinear fiber samples with different taper radius and numbers of PAH/PB bilayers. We note that even with 40 bilayers of nonlinear film, the transmission loss through the entire taper region is 5-7 dB. The transmission loss can potentially be further lowered by reducing the number of dust particles attached to the fiber taper [27].

3. Experiments and results

The nonlinear optical properties of the fiber taper are characterized through second harmonic generation. As shown in Fig. 2, an OPO is used to generate linearly polarized pump pulses at 1294 nm. The pulse width is 10 ns with a repetition rate of 20 Hz. The pump pulse energy is adjusted by rotating the polarizer (P1) and measured using an optical power meter. (The power meter will be removed when we perform SHG measurements.) Two long-pass filters (F1 and F2) are used to remove background second harmonic signals generated by the polarizer and other optical components (e.g., any surface SHG signals). The pump light is coupled into a multimode fiber and transmitted through a nonlinear taper region. The second harmonic signals generated by the nonlinear taper are confined within the silica core and coupled back into the multimode fiber. At the fiber output, both the fundamental pump and the second harmonic signal are collimated back into free space, where we used a short pass filter (F3) to remove the pump light. The wavelength of the second harmonic signal is verified by a monochromator, and its power is detected by a photomultiplier tube (PMT). To eliminate any inconsistency in coupling free space optical signals in and out of the silica fiber, the entire fiber collimation systems, which consists of multiple lenses and translation / rotation stages,

are kept unchanged during the measurement processes. Different nonlinear fiber samples are connected with the multimode fiber through fiber splicing. The total splicing loss is consistently kept at the level of less than 0.01 dB.
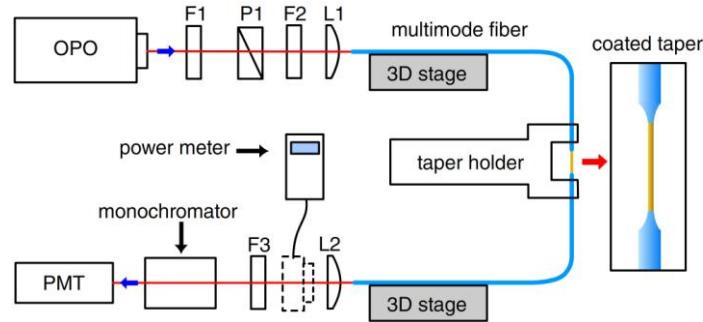

Fig. 2. Schematic diagram of the experimental setup. An infrared, nanosecond-pulsed pump beam obtained from an OPO system is coupled into a multimode fiber. The beam propagates through a nonlinear taper, and interacts with the second-order nonlinear molecules on the taper surface. The output SHG signal is collimated, filtered and finally detected by a PMT.

Previous work [28,29] suggests that common silica fibers may exhibit weak second-order nonlinear responses (e.g., SHG and SFG) if pump peak power reaches the level of 100 kW. To eliminate such effects, we limit the peak power of our pump pulses to 400 W and below, and keep the total length of the multimode fiber to be 2 m or less. Furthermore, we quantify the background SHG signal strength by bypassing the nonlinear taper in Fig. 2 and directly splicing the two sections of multimode fiber together. Under the aforementioned experimental conditions, the background SHG signals of our measurement system cannot be detected. Furthermore, by using a moderate pump power, we can avoid the problem of optically damaging the self-assembled organic film through undesirable effects such as photobleaching at high pump intensity.

We first verified the existence of SHG by measuring the spectrum of nonlinear optical signal generated by a nonlinear fiber sample. Figure 3 compares the spectra produced by a fiber taper (waist radius: 3.8 µm) before and after coating with the self-assembled PAH/PB films. For the bare fiber taper (i.e., without nonlinear coating), the measured spectrum clearly contains both a second harmonic component at 647 nm and a third harmonic component at 431 nm. The 431 nm component is due to third harmonic generation (THG) [30,31], which is further confirmed by the measurement of the THG power as a function of pump pulse energy, as shown in the Fig. 3 inset. The small second harmonic component produced by the bare fiber taper can be attributed to SHG at the air-silica interface in the taper region [32]. After coating the same fiber taper with 10 bilayers of PAH/PB film, we note that the third harmonic signal becomes much weaker. (The reduction in THG power can be attributed to the strong PAH/PB absorption at 431 nm, as indicated in the inset of Fig. 3.) The second harmonic signal produced by the PAB/PB-coated nonlinear fiber, on the other hand, becomes much stronger.
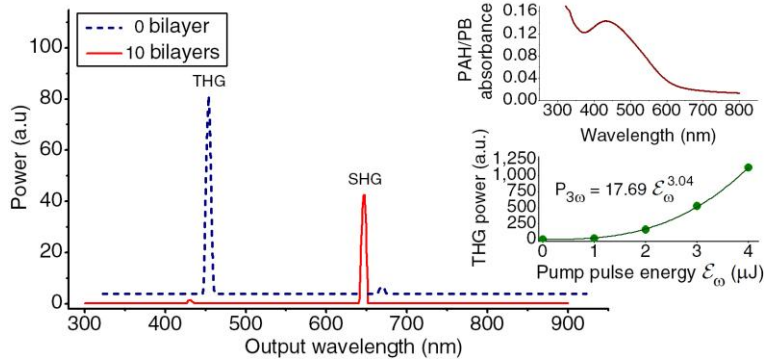
Fig. 3. The THG (at 431 nm) and SHG (at 647 nm) spectra from a bare and a 10-bilayer coated taper, excited by pump pulse energy of 2 µJ at 1294 nm. The bare fiber curve is shifted both vertically and horizontally for clarity. The lower inset confirms a cubic dependency of the THG emitted from the bare taper. With nonlinear coating, we observe an increase in SHG power and decreased THG component due to the film absorption at 431 nm as indicated in the upper inset.

To further clarify the origin of SHG, we measured the dependence of SHG power on pump pulse energy using several nonlinear fiber samples. To remove pump polarization dependence, all pump light is linearly polarized, as indicated by our optical system in Fig. 2. To eliminate variations due to different taper geometries, all nonlinear fiber samples were fabricated from the same bare silica taper used in Fig. 3. Our procedure is as follows: We first performed SHG measurement on the bare silica taper followed by depositing 10 bilayers of PAH/PB film on the bare taper. We then performed the SHG measurement again followed by adding 10 additional bilayers of PAH/PB coating. This SHG measurement / film deposition cycle was repeated until we reached 40 bilayers of PAH/PB film. As shown in Fig. 4, we notice that second harmonic power increases quadratically as a function of the pump pulse energy, a characteristic feature of SHG. Furthermore, an increase in nonlinear film thickness directly leads to an increase in second harmonic power. For a 40-bilayer coating, we observe a 400-fold increase in SHG power compared to the bare taper case. These results confirm that the measured second harmonic component is indeed generated by the nonlinear PAH/PB coating.
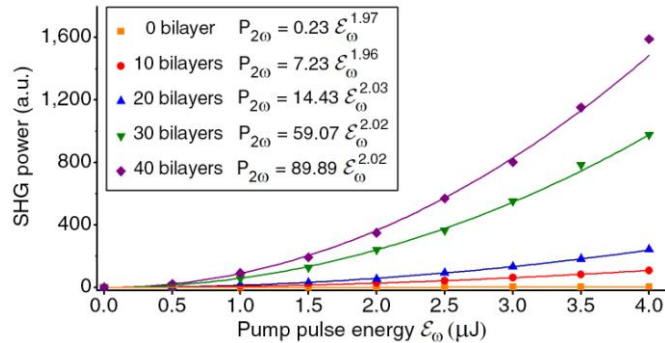

Fig. 4. SHG power as a function of pump pulse energy. The measurement was taken for a 3.8-µm-radius taper with 0, 10, 20, 30 and 40 bilayers of nonlinear film. Each data point is the result of an average of over 100 measurement data and the error bar is smaller than the symbol. The lines are quadratic fits to the data.

The dependence of SHG power with taper waist radius was also studied and the result is shown in Fig. 5. The SHG data was collected from five nonlinear fiber samples with waist radii varying from 2.8 µm to 7.5 µm. All samples are coated with 10-bilayer PAH/PB film, and all SHG measurements are performed using a 1294 nm pump with pulse energy of 2 µJ per pulse (peak power of ~200W). The log-log plot for SHG power versus taper radius is

shown in Fig. 5 and clearly reveals $1/a^4$ behavior (where a is waist radius), which is consistent with our previous theoretical prediction reported in Ref [21]:

$$P_{2\omega} = 2\omega^2 \left(\frac{\mu_0}{\varepsilon_r \varepsilon_0}\right)^{3/2} \frac{P_\omega^2}{\pi a^2} \left|\frac{\delta}{a} \chi_{zzz}^{(2)}\right|^2 L^2 \times \frac{\sin^2(\Delta\beta L/2)}{(\Delta\beta L/2)^2} \tag{1}$$

In Eq. (1), P_ω is the power of fundamental beam, $P_{2\omega}$ is the power of SHG, ω is the angular frequency of fundamental beam, δ is nonlinear film thickness and L is the taper length (a constant taper waist is assumed). The last term of the equation accounts for phase mismatch between the fundamental and the second harmonic mode, with $\Delta\beta = 2\beta_1 - \beta_2$, where β_1 and β_2 are respectively the propagation constants of fundamental beam and its second harmonic. Equation (1) predicts a $1/a^4$ power dependence as well as fluctuations due to phase mismatch [i.e, the $\sin^2(\Delta\beta L/2)$ term]. Both effects are visible from Fig. 5, where we can observe a general trend of $P_{2\omega} \propto 1/a^4$ as well as a small variation around the $1/a^4$ fitting line.
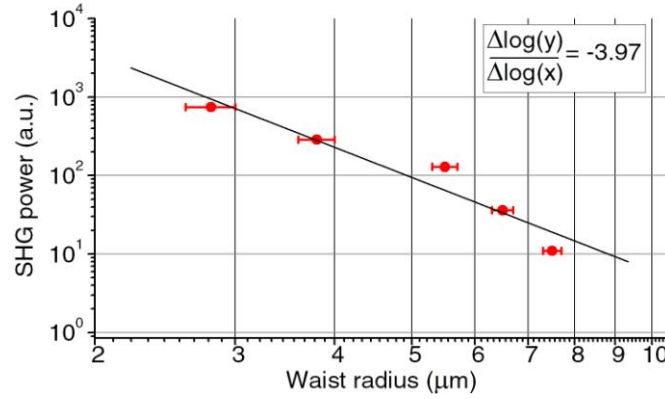

Fig. 5. Dependence of SHG on taper radius. The log-log plot shows the $1/a^4$ behavior of SHG power with different taper radius. All samples are coated with 10-bilayer films and excited with pulse energy of 2 μJ. The error bars in the x axis indicate the estimated accuracy of taper radii measurements (± 0.2 μm) as determined by the optical microscope.

An additional study of the impact of phase mismatch was carried out as follows. To account for the effect of non-uniform taper profile, we follow the procedure in Ref [21]. and obtain a coupled mode equation for SHG in the nonlinear taper:

$$\frac{dE_{2\omega}}{dz} = -i \frac{\omega E_\omega^2}{\varepsilon_0 \upsilon_g} \frac{\delta}{\sqrt{\pi} \varepsilon_r^{3/2} a(z)} \chi_{zzz}^{(2)} e^{-i\Delta\beta(z)z}, \tag{2}$$

where E_ω and $E_{2\omega}$ are respectively the electric field amplitude of pump and SHG beams, and υ_g is group velocity at 2ω. (We choose the propagation distance z such that the narrowest fiber taper radius is at $z = 0$.) In Eq. (2), the only parameter that cannot be readily obtained from experimental conditions is the phase-mismatch term: $\Delta\beta = 2\beta_1 - \beta_2$. To calculate this term we assume the fundamental waves are in the HE_{11} mode. This assumption is based on the observation that fiber taper transition is gradual and smooth, which should minimize the excitation of higher order modes such as the HE_{12} mode. This assumption is verified by monitoring the transmission of optical power during the taper pulling process. Figure 6(a) shows the transmission coefficient as a function of taper pulling time. At the end of taper pulling, the fiber taper radius is approximately 0.5 μm, which is less than the cutoff radius for the HE_{12} mode (0.6 μm at wavelength 980 nm, assuming a fiber with silica core and air

cladding). The absence of significant higher order mode coupling is confirmed by the high transmission (T > 90%) throughout the entire taper pulling process.

We can use Eq. (2) to theoretically estimate the efficiency of second harmonic generation. For linearly polarized pump light, the second harmonic mode can be either HE_{21} or TM_{01} mode [21]. In deriving Eq. (2), we have utilized a few simplifying assumptions in Ref [21]. to remove azimuthal dependence. In the final result, i.e., Eq. (2), the choice of either picking HE_{21} mode or TM_{01} mode only impacts a single parameter: $\Delta\beta$. For our present study, in which the taper size is several microns, we found that the propagation constants of the HE_{21} and TM_{01} mode are very close. In fact, as shown in Fig. 6(b), the difference between the propagation constant of the HE_{21} and TM_{01} mode is of the order of 10^{-5} or less. Therefore, for the purpose of an order-of-magnitude estimate of second harmonic power, whether we choose HE_{21} or TM_{01} as the second harmonic mode should not make a significant difference.
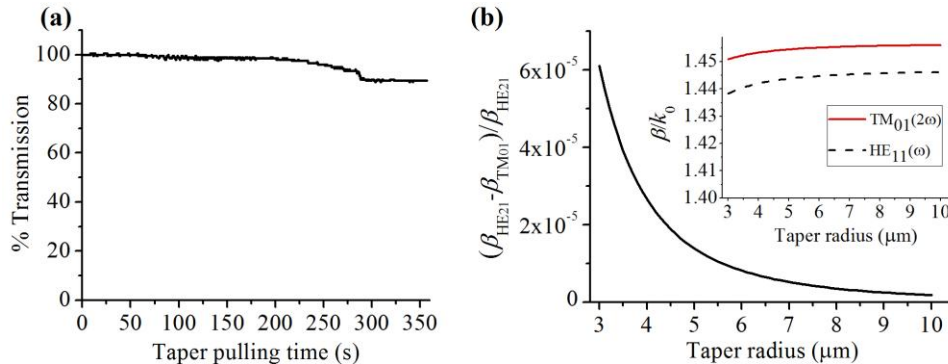

Fig. 6. (a) Typical real-time transmission of optical power (at 980 nm) during the taper pulling process. The taper pulling was stop at the taper radius ~0.5 μm. (b) The difference between the propagation constants of the TM_{01} mode and HE_{21} mode at the SHG wavelength of 647 nm. The inset shows the propagation constant of the TM_{01} (at 647 nm) and HE_{11} mode (at 1294 nm).

We then used an optical microscope to obtain an image of the entire fiber taper region as shown in Fig. 7(a). Then, using a Matlab program, we converted the microscope image to a binary bitmap, from which we extract fiber radius at any given location. Using this method, we obtained radial profiles of five different fiber tapers. We then compared waist radii obtained using this method with those directly measured from SEM images. For all five samples, the difference between the two approaches is less than 0.2 μm, which is at the resolution limit of an optical microscope.

Following the above assumptions on the propagating modes and using the fiber waist profile extracted from the optical microscope image, we can numerically calculate the value of $\Delta\beta(z)$ as a function of propagation distance z. Once the $\Delta\beta(z)$ is known, we can then numerically integrate Eq. (2) and obtain the power of second harmonic wave. In Fig. 7(b), we perform numerical integration starting from $z = -L/2$ to $z = L/2$ with various values of interaction length L, and plot the second harmonic power as a function of the interaction length L. We note that $P_{2\omega}$ in Fig. 6(b) converges to a finite result for L greater than 3000 μm. Therefore, we consider $L = 3000$ μm to be the effective interaction length that defines the region of strong interaction between nonlinear molecules and the pump field. This observation is also consistent with the taper profile shown in Fig. 7(a), where, at $z = \pm 1500$ μm, taper diameter grows to approximately twice of its waist value. The simulation result in Fig. 7(b) also agrees reasonably well with experimental data: For a peak pump power of 400 W at 1294 nm, the numerical integration indicates that we should expect a SHG power of 169.7 μW, whereas the experimentally measured second harmonic peak power is 49.8 μW. The agreement is reasonable, especially considering the fact that the numerical estimate is obtained without using any empirical fitting parameters.
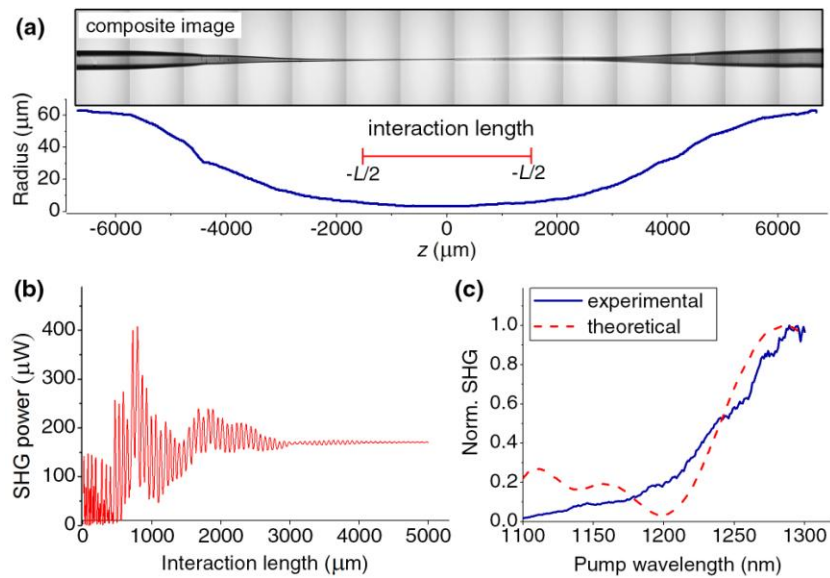
Fig. 7. (a) The profile of a 3.8-μm taper obtained by combining sequential images taken using an optical microscope (Leica DMI-6000 B). (b) Theoretical estimate of SHG power as a function of taper interaction length. The result is obtained by numerically integrating the coupled mode Eq. (2) while using the taper profile determined in (a). (c) Theoretical simulation and experimental result of SHG power versus pump wavelength. Both results are normalized with respect to their corresponding peak SHG power.

By following the procedure outlined above and using parameters extracted from the actual nonlinear fiber, we can also calculate the strength of second harmonic signal generated by the nonlinear fiber as a function of pump wavelength. (The pump peak power is fixed at 400W.) The numerical result is shown in Fig. 6(c) as a dashed line. The corresponding experimental result was obtained by tuning the OPO pump wavelength from 1100 nm to 1300 nm with a wavelength step of 1 nm. The pump power was maintained constant throughout the wavelength scan. At any given pump wavelength, the monochromator is adjusted so that only second harmonic light can pass through and be detected by the PMT. The experimentally measured SHG power is shown in Fig. 7(c) as a solid line. Again, we observe good agreement between the theoretical prediction and the experimental results. The small discrepancy between the theoretical predictions and the experimental results in the shorter wavelength region can be attributed to the absorption of the second harmonic signal by the PAH/PB film. This absorption of nonlinear molecule is due mainly to their electronic excitation, and it is generally a trade-off between short wavelength in which the molecules are transparent and the magnitude of $\chi^{(2)}$. There are extensive studies on molecular design and synthesis for second–order nonlinear chromophores that can simultaneously provide large nonlinear coefficient and exhibit low optical absorption at the desired wavelength [33].

The nonlinear fibers we have considered so far are not phase matched for SHG, which limits their nonlinear conversion efficiency. Quasi phase matching can be possibly achieved by periodic coating of nonlinear film with period $\Lambda = 2l_{coh}$ (where l_{coh} is the coherence buildup length for the SHG power). For the taper shown in Fig. 6, the coherence buildup length l_{coh} is approximately 25 μm. Several fabrication techniques are promising to produce such a periodic structure of nonlinear film on a taper surface, e.g., laser ablation on the film surface using phase mask [34], direct electron-beam patterning [35], and photochemical patterning [36]. Furthermore, intermodal phase matching can be accomplished by adjusting taper radius down to submicron scale [37]. For example, with a taper radius of 0.288 μm, the fundamental pump at HE_{11} mode and the second harmonic signal at TM_{01} mode is phase matched at the wavelength 1294 nm (or the taper radius of 0.322 μm is required for SHG in HE_{21} mode).

Under the intermodal phase-matching condition, a 100-µm-long nonlinear fiber with 40 bilayers of PB/PAH coating can achieve 10% SHG efficiency with a pump peak power of 400 W. Work in this direction is currently in progress. Finally, we point out that the cutoff radii for TM_{01} and HE_{21} mode are 0.235 and µm 0.269 µm (at pump wavelength of 1294 nm), respectively. Therefore, for any given pump wavelength, there is a lower limit on taper size, below which we should not observe any significant second harmonic generation.

4. Conclusion

We have experimentally demonstrated that a cylindrically symmetric nonlinear fiber can exhibit significant second order nonlinearity. The nonlinear fiber is fabricated utilizing a hybrid covalent/ionic self-assembly technique and is thermodynamically stable. Despite the overall rotational symmetry of the nonlinear fiber, we have observed significant second harmonic generation. We can attribute the SHG to the radially aligned nonlinear molecules, and have obtained good agreement between theoretical predictions and experimental measurements. Further improvement in nonlinear conversion efficiency can be obtained by achieving phase matching using different methods in current literature.

Acknowledgements